NUMERICAL-EXPERIMENTAL VALIDATION OF THE WELDING THERMAL CYCLE CARRIED OUT WITH THE MIG WELDING PROCESS ON A 6063-T5 ALUMINIUM TUBULAR PROFILE

by

José L. Meseguer Valdenebro[a1], Eusebio J. Martínez-Conesa[b], Antonio Portolés[a]

[a] Department of Applied Physics and Materials Engineering, School of Mechanical Engineering, Technical University of Madrid, C/José Gutiérrez Abascal St, 2, 28006 Madrid, Spain

[b] Departamento de Tecnología de Edificación, Universidad Politécnica de Cartagena (UPCT), Pza. del Cronista Isidoro Valverde, Edif. La Milagrosa, 30202 Cartagena, Spain

The purpose of this work is to validate the thermal welding cycle obtained experimentally with the MIG welding process on a 6063-T5 aluminium tubular profile using the finite element method. The assembly formed by the tubular profile and the weld bead obtained experimentally is represented in an accurate way, taking care of both the geometry and the contour of the weld bead. The precision achieved in the numerical-experimental validation carried out by means of the finite element method is due to the care that has been taken in drawing the welded piece together with the weld bead made experimentally. In the validation carried out, the experimental and numerical cooling curves and the critical cooling time between 400 and 300 ºC ($t_{4/3}$) in both curves are compared.

Keywords: weld; simulation; ANSYS; $t_{4/3}$; cooling time

1. Introduction

1.1 Background on the thermal welding cycle of aluminium alloys

The thermal welding cycle allows the mechanical properties to be obtained in the joint [1–4]. If these properties obtained in the joint present soft structures, the aluminium weld will be thermally treated at high temperatures between 400 and 500 ºC [5] for a determined time, causing precipitates in its matrix, which dissolves again, producing a solution that is rich in solute. The solution processes

[1] Corresponding author; e-mail: jlmeseguer507@gmail.com

increase the concentration of hardening elements in the alloy, including copper, zinc, magnesium, or silicon in the solid solution [6]. The concentration and the dissolution ratio of these elements increase while the precipitate is kept at a constant temperature for a certain time; in this way, the temperatures in the solution treatments are generally close to the liquid line on a dissolution diagram [7]. If an aluminium alloy is abruptly cooled from a high temperature, the alloy elements that the alloy contains precipitates in its interior, becoming concentrated at the edges of the grains, with a greater presence in small cavities of the crystalline structure, in dislocations, and in other types of imperfections in the crystalline structure of the aluminium [8]. To achieve optimum toughness, hardness, and corrosion resistance, the diffusive process must be delayed and the elements must be maintained in solid solution until the alloy hardens with time (ageing) [9]. Once it has cooled, the aluminium presents a degree of ageing [10]. This is represented in the microstructure by the presence of a fine dispersion of elements and compounds that precipitate, which significantly increases the toughness of the material [11].

The thermal cycle of aluminium alloys is defined by the critical cooling time between 400 and 300 ºC, also known as $t_{4/3}$ [12], and depending on the duration of $t_{4/3}$, the welded joint presents particular degrees of ageing and mechanical resistance. The critical temperature range is defined as the range of temperatures that produces the biggest precipitate ratios [13]. The average ratio of critical cooling is determined by calculating the time needed to cool the piece from 400 ºC down to 300 ºC. This critical time is represented by $t_{4/3}$ and determines the quality of the welded joint at the time of cooling. Fig. 1 shows the intersection between the cooling curve obtained with the MIG welding process for 6063-T5 aluminium alloy and the TTP curve of the same alloy [14]. On the cooling curve, the cooling time $t_{4/3}$ is shown; this is the critical cooling time between 300 and 400 ºC at which nucleation takes place. The area of intersection between the cooling curve and the TTP curve qualitatively represents the precipitates that appear in the joint [15].

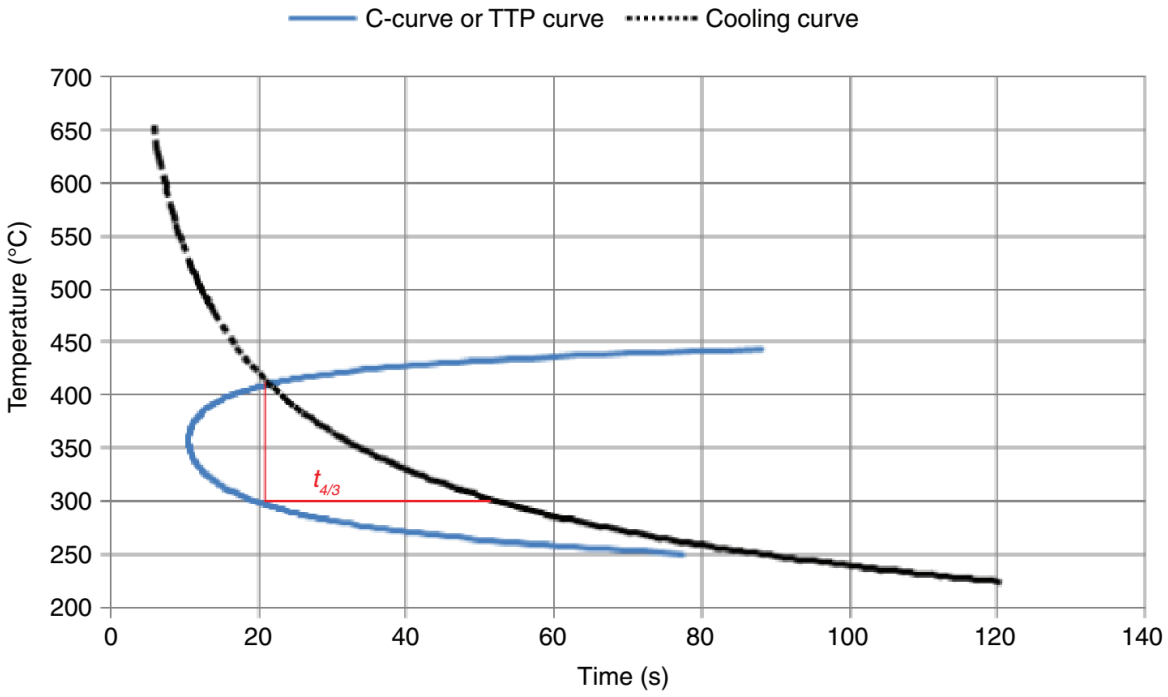

Fig. 1. Determination of the cooling factor by combining the cooling curve and the C-curve [12]

1.2 Studies that determine the welding cycle by means of numerical methods.

The basic theory of heat flow was developed by Fourier. Rosenthal [16] and Rykalin [17] applied it to a source in movement. More recent studies [18–20] have achieved values of heat contributed by the source which better approximate reality, with greater calculation accuracy. To achieve the improvement in the calculation accuracy, programs have been used that employ the finite element method to represent the heat distribution on a surface [21–24]. Studies carried out by Pavelic *et al.* [25] supposed that the distribution of the heat source would have a Gaussian shape, with the heat-affected zone taking a disc shape. The Pavelic disc model was optimized by Paley [26], who used a constant density heat source to define the shape of the fusion zone by the finite difference method, but the length of the melted zone was not shown. Finally Goldak *et al.* [27], by means of the double-ellipsoid model, obtained a source size with an ellipse shape.

Those were the first studies carried out on a heat source in movement and the welding cycle. The most frequently used model is the Goldak model [28], which allows the welding cycle to be obtained from the parameters of the Goldak double ellipsoid, and by estimation of the source size, the welding cycle of the welded joint is obtained, but the shape of the weld bead is not taken into account, as will be done in the present work.

2. Experimental procedure

The objective of the empirical procedure is to form a joint by electric arc welding on 6063-T5 aluminium alloy and to validate it by means of the finite element method developed.

2.1. Materials and means

2.1.1 Base Material

The empirically assayed material is 6063-T5 aluminium. The fusion point for this aluminium is estimated to be 655 ºC and the chemical composition of the aluminium alloy tested is indicated in Table 1. The physical properties of the 6063-T5 aluminium alloy according to temperature are shown in Table 2.

Si	Fe	Cu	Mn	Mg	Cr	Zn	Ti
0.20–0.60	0.35	0.10	0.10	0.45–0.90	0.10	0.10	0.10

Table 1. Composition in wt% of the 6063-T5 aluminium alloy

Temperature (ºC)	*K, W/mºC*	*cp, J/kgºC*	Density, kg/m^3
25	191.75	913.25	2680
38	192.66	918.58	
65	194.55	929.65	
80	195.6	935.8	2669
93	196.51	941.13	
121	198.47	952.61	
149	200.43	964.09	
177	202.39	975.57	
180	202.6	976.8	2651
204	204.28	986.64	
240	206.8	1001.4	

280	209.6	1017.8	2634
330	213.1	1038.3	
380	216.6	1058.8	2616
400	218	1067	
430		1079.3	
480		1099.8	2598
500		1108	

Table 2. Properties of the 6063-T5 aluminium alloy [29]

Fig. 2 shows the tubular 6063-T5 aluminium used as the base metal to form the welded joint. The tube has a length of 150 mm, exterior diameter of 50 mm, and thickness of 2 mm. The tube used to carry out the welding is cut into two equal halves, without preparation of the edges, with the aim of subsequently welding them to each other on one side. The gap between the edges to be joined is 0 mm.

Fig. 2. Tube of 6063-T5 aluminium employed as base metal

2.1.2. Welding procedure

The welding procedure used is electric arc welding with inert gas protection (argon 99%) and an ER-5356 electrode, using the *MIG* welding technique. Commercial argon P-4563, supplied by Praxair, is selected as the protection gas. The gas flow used is 14 l/min., and the welding is carried out with AW 5.10 ER-5356 filler material [30], whose composition is given in Table 3. The welding is carried out in PA position [31], equivalent to the horizontal position under European regulations. The electrode used has a diameter of 1.2 mm and its fusion point is between 574 and 632 ºC, similar to that of the base metal, whose chemical composition is given in Table 3. The type of current selected is continuous with inverted polarity. The zone of the welded joint is superficially prepared with a stainless-steel metal brush to eliminate any type of surface oxidation that would complicate the stability of the electric arc during the welding. Finally, to eliminate any possible remaining dirt from the base material, the zone to be welded is cleaned with nitric acid at 68% and water for 30 seconds in order to eliminate the layer of oxides on the surface of the base metal. Due to the thickness of the plate, the welding could be performed without preparing the edges.

Mn	**Si**	**Ti**	**Cu**	**Mg**	**Zn**	**Be**	**Fe**
0.05	0.25	0.06	0.10	4.5	0.10	0.0008	0.4

Table 3. Chemical composition of the ER-5356 filler material (wt%)

2.2 Equipment used for welding and thermographic camera

This section details the experimental equipment used to carry out and analyse the welded joints.

2.2.1. Welding robot

An ABB six-axis robot, model IRB 1400, which was designed specifically for arc welding, is used to carry out the experimental study of the welding parameters. The welding processes for which adaptable torches are available are MIG and *GTAW*. The torch used in the experiments is the *MIG* head. Fig. 3 shows an image with the complete distribution in the welding workshop of the welding and measuring equipment and the consumables used to form the welded joint.

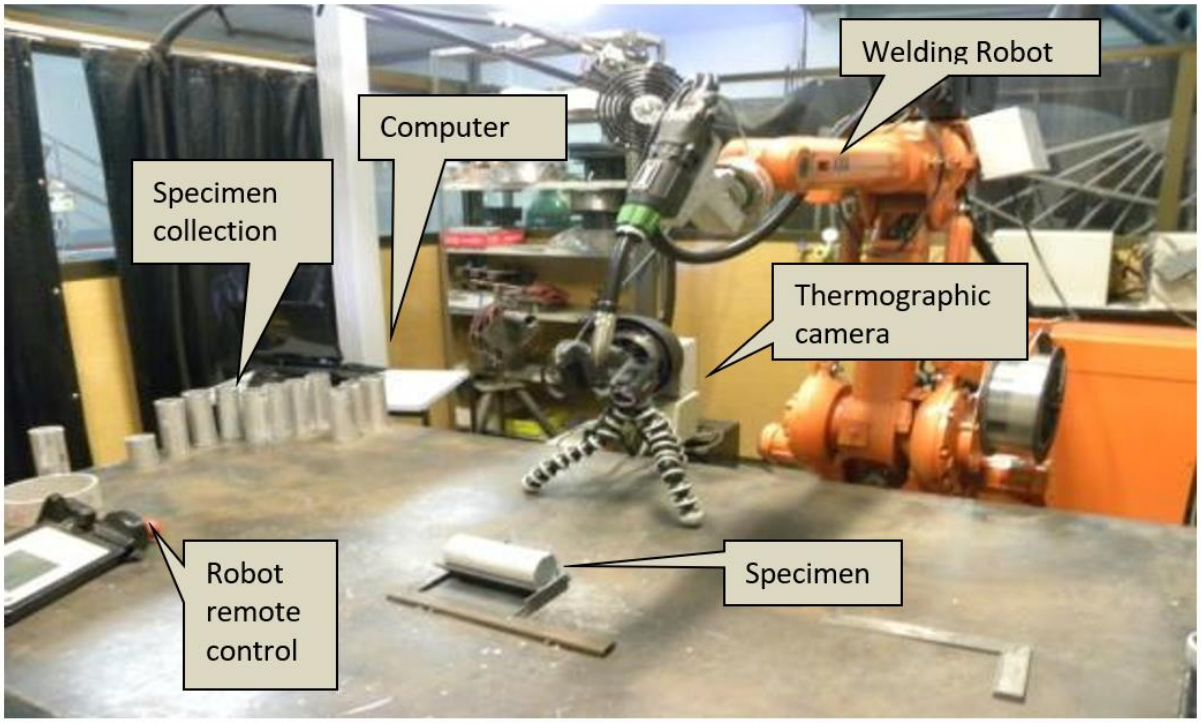

Fig. 3. Scheme of the power source, welding arm, and thermal camera.

2.2.2. Thermographic camera

The thermographic unit measures the temperature distribution in the piece once it has been welded; the camera model is FLIR T440.

The FLIR T440 thermographic camera is connected by USB cable to a laptop computer to record the welding thermal cycle. The thermographic camera has been calibrated for the 6063-T5 aluminium alloy with thermocouples placed on another welded piece with similar characteristics to those used in the test. Fig. 4 shows the temperatures reached in the weld when the weld bead has just been finished.

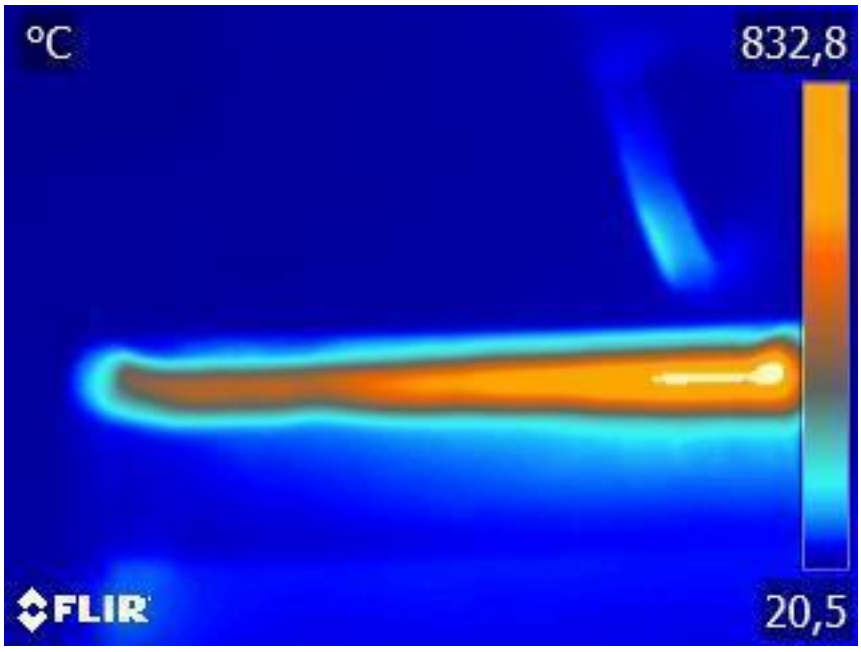

Fig. 4. Welding image obtained by FLIR thermal imaging camera

2.2.3. Welding tooling

For the purpose of supporting the tubes in a horizontal position, a carbon steel tool has been designed: it is V shaped, 150 mm long, and connected to a horizontal bar that supports the tube, restricting its movement in the moment of welding. The form of this tool is represented in Fig. 5.

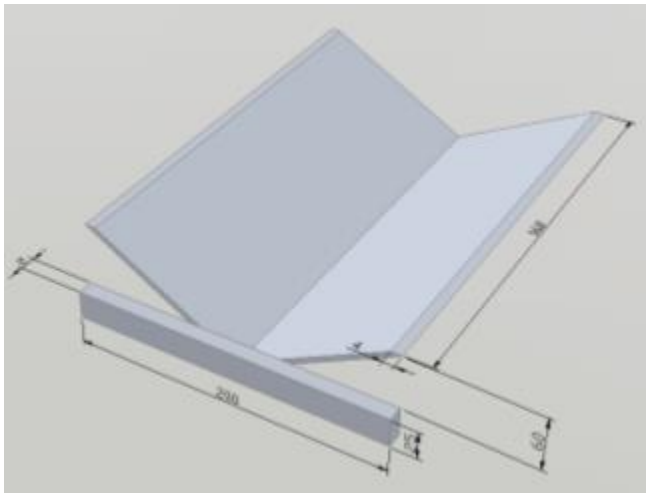

Fig. 5. Tool used for the welding of the specimen.

2.3 **Experimental results obtained**

There are a wide variety of works where the thermal cycle of welding is studied from an experimental point of view and from a numerical point of view. Below are some of the most relevant cases.

Mato *et al.* [32] performed an experimental numerical validation for a T joint, where the deformations of the welded profiles and the thermal cycle of the weld were studied. A work with greater depth of detail was carried out by Deng *et al.* [33], where the deformations of a T-profile due to the thermal

cycle of the welding were evaluated. Segarra and Portolés [34] evaluated the properties of magnesium alloys by modelling the finite element thermal cycle and the thermally affected area.

Ivanovic *et al*. [35] performed a numerical study on the displacement of the heat source in the three main directions of space. Bjelic et al. [36] performed a study similar to the previous one, but considering the two dimensions of space.

Of all the works presented, we have not found any work that has performed a study where the longitudinal welding on a tubular profile is analysed, taking into account the geometry of the weld bead with the precision that has been achieved in this work. The thermal model, from a mathematical point of view, is the same as that used in the aforementioned works, but in those works the geometry of the weld bead was not taken into account as an input as it has been in this publication.

2.3.1 Welding parameters

The welding parameters used are as follows.

Fixed parameters	**Units**	**Value**
Protection gas flow (argon 99%)	*l/min*	14
Variable parameters	Units	**Value**
Voltage	*V*	17.3
Intensity	*A*	90
Welding speed	*mm/s*	11.5
Separation of edges between profiles	*mm*	0.0

Table 4. Parameters of the experiment

2.3.2 Profile of the experimental weld bead

The main measurements of the weld bead are delimited in order to enable their shape to be exported to the numerical model and perform the corresponding analysis. The shape of the weld bead obtained and the principal dimensions of the weld bead are shown in detail in Fig. 6.

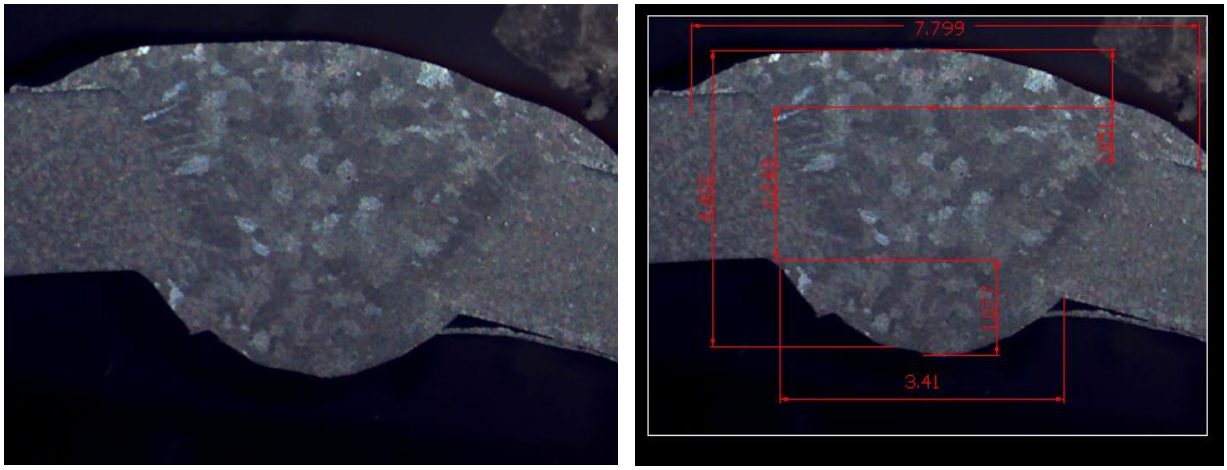

Fig. 6. Weld bead obtained in the welding process. Units in millimetres

In Ref. [37], the geometry of the weld bead shown in Fig. 6 was studied in detail using the design of experiments; that is, the representation of the weld bead was analysed in detail in the reference cited in this paragraph.

2.3.3 Experimental welding thermal cycle

The thermal cycle of the weld bead performed is measured with the thermographic camera, which has been previously calibrated. The thermal cycle of the weld obtained experimentally is shown in Fig. 7. The critical cooling time $t_{4/3}$ obtained experimentally is 4,4 seconds. The temperatures obtained experimentally in the welding correspond to the highest temperature reached, that is, in the last stretch of the weld bead.

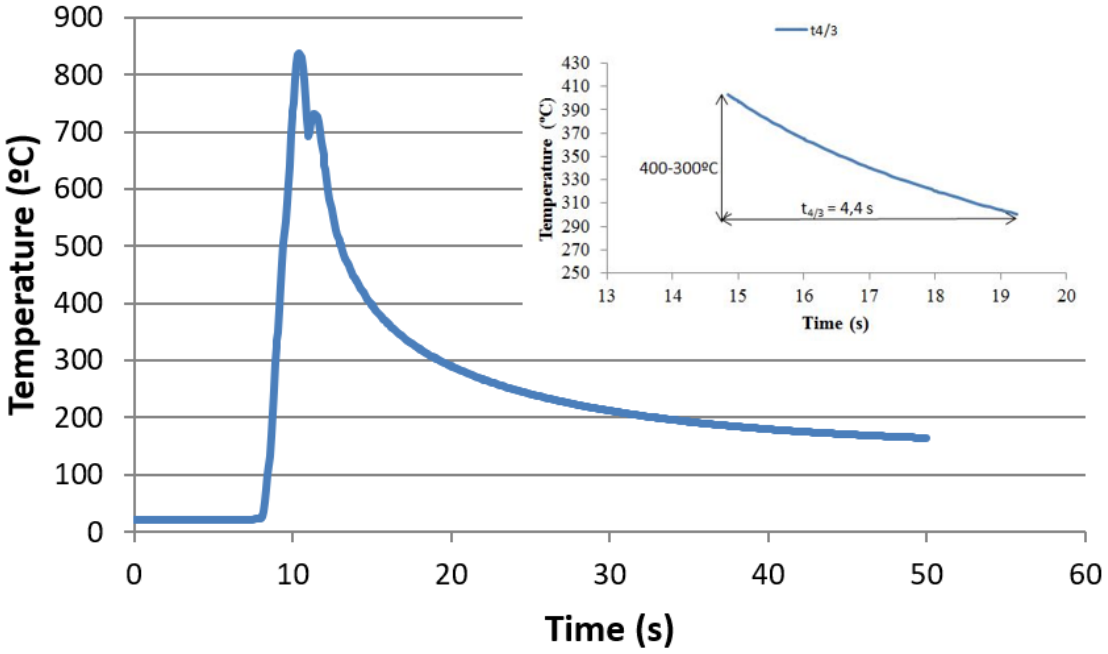

Fig. 7. Thermal cycle obtained experimentally

As can be seen in Fig. 4, the hottest zone of the weld corresponds to the end of the pipe, when welding is finished. The heat source has advanced along the pipe and the heat tends to dissipate along the pipe in the direction of the point where it began to weld. When welding is finished, there is an accumulation of heat at the end of the piece, and therefore this is the hottest area, where the curve of the thermal cycle of the weld will be measured.

Fig. 7 shows the measurements the thermal cycle for the time instant of 10 seconds, it has been verified by the measurements of the thermal camera that there are no variations for the time instant of 13 seconds, that is, when the welding finishes, taking into account that the advance speed is 11,5 mm/s and the length of the tube is 150 mm.

3. Numerical procedure

3.1 Modeling the welding set

The geometry of the weld bead and the base metal used are modelled in ANSYS. Fig. 8 shows the finish of the welded set modelled prior to the numerical analysis.

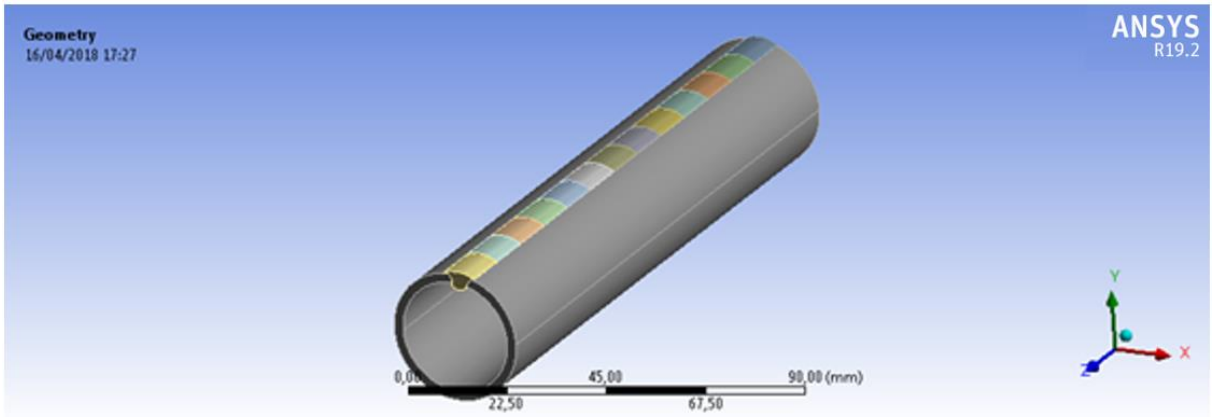

Fig. 8. Modelling of the welded set

The central body of the tube is a single piece, but the weld bead is divided into several parts proportional to the welding speed for one second of time; that is, each of the parts that make up the weld bead measures 11,5 mm and is represented by a different colour in Fig. 8. The properties of both the base metal and the weld bead are the same and are as presented in Table 2. The temperature is measured at the time instant of 10 seconds, that is, in the tenth section of the weld bead.

It is checked that the geometry of the numerically modelled weld bead is very similar to the geometry of the weld bead obtained experimentally.

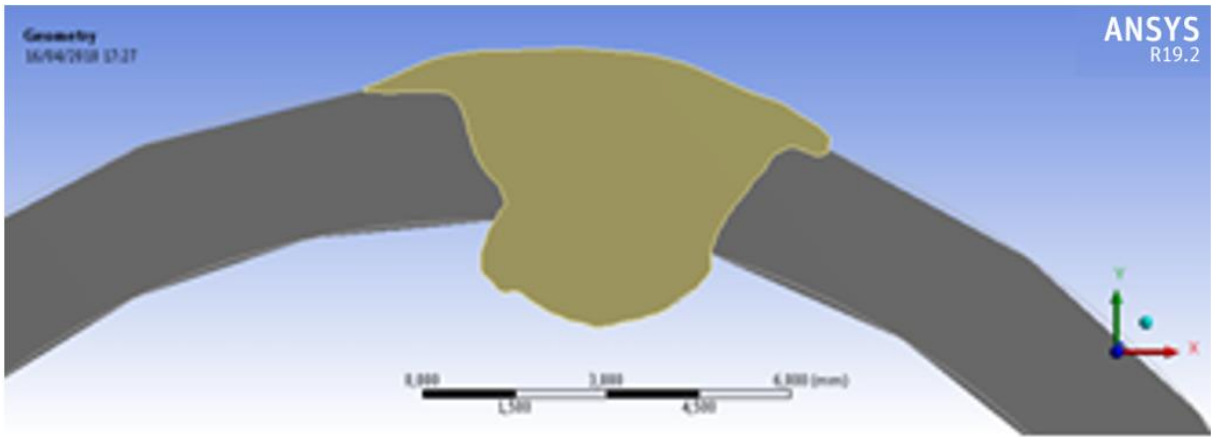

Fig. 9. Weld bead modelled in ANSYS

To obtain this high level of similarity between the numerical weld bead and the experimental one, the weld bead has been defined by means of an iso-line and the points have been extracted taking the dimensions of the bead that appear in Fig. 6 as the reference. The points have been extracted using the open-source program Data-Thief.

3.2 Meshing

Meshing has been done using the element SOLID 90, which is used by default in ANSYS for transitory thermal analysis. The mesh size is 1 mm for the weld metal and 2 mm for the base bead; that is, it is a degraded matrix, where the finest mesh is located in the weld bead where the heat source is going to move. The size of the mesh made has been evaluated by a mesh sensitivity analysis, and it has been determined that the appropriate size for a stable temperature result and $t_{4/3}$ corresponds to the indicated mesh value. The meshed welding set is shown in Fig. 10 with a total of 12084 elements and

66489 nodes, taking into account that the length of the tube is 150 mm. Although the geometry of the bead is complex, ANSYS has an option that allows the mesh to be carried through the geometry edge, tracing the weld bead, guaranteeing a high-precision mesh.

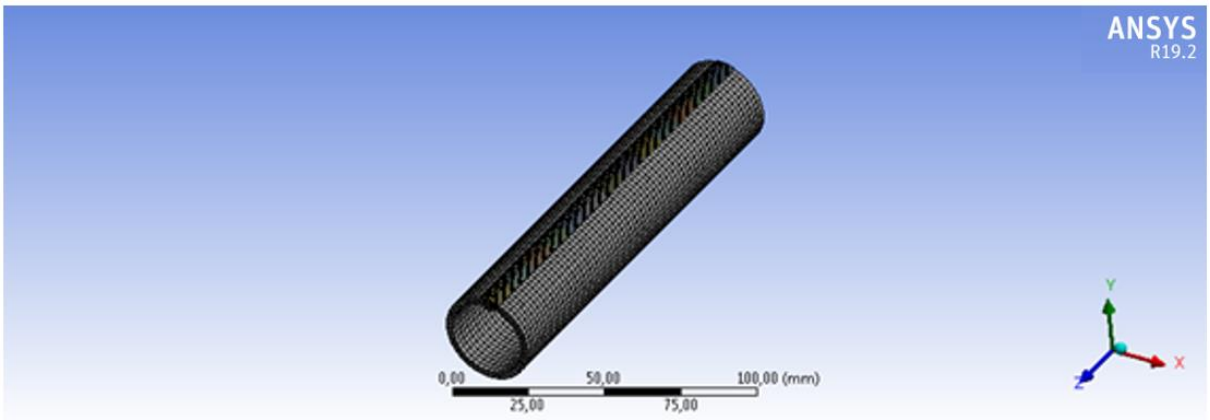

Fig. 10. Meshed welding set.

3.3 Loads applied

Different types of loads can be applied in a thermal model, such as temperature, heat generation, heat flow, convection, and radiation, principally. For this model, different types of loads are applied: heat generation, convection, and radiation on the surface of the bead and the base metal and an atmospheric temperature of 22 ºC, which corresponds to room temperature.

- **Heat-generating elements**

The bead elements are heat-generating elements. The heat-generating elements in a transitory regime provide the heat flow of the process. The thermal loads applied along the weld bead are measured in watts per cubic metre and are obtained by dividing the power that the source contributes by the bead volume in each instant of time. The bead volume for each second is equal to $2{,}1386 \cdot 10^{-7}$ m^3/s. Therefore, the power per second for each 11.5 mm of welding is equal to $5{,}8972 \cdot 10^{9}$ W/m^3.

The power applied is equal to the product of the thermal yield of the process multiplied by the parameters of the source, which are the intensity I and the voltage V, divided by the source advance speed. The thermal efficiency of the MIG process is equal to 0,8 [38].

- **Convection and radiation**

Modelling of the heat transfer by convection and radiation is performed through the surfaces of the model. The convection applied is $5*10^{-6}$ W/mm^2 ºC and the radiation has an emissivity for the aluminium equal to 0.7 in melted state [39].

The heat losses through radiation and convection are applied on the surfaces of the tube and are taken into account through the following relationship [15]:

$q_c = h(T - T_\infty)$ (Eq. 1)

$q_r = \varepsilon\, s\, (T^4 - T_\infty^4)$ (Eq. 2)

where h (W/m^{2}ºC) is the convection coefficient, T_{∞} (ºC) is the environmental temperature, ε is the body surface emissivity, and s is the Stefan-Boltzmann constant. The initial conditions are 25 ºC in the whole of the model.

3.4 Results obtained

The numerical results obtained are described below.

3.4.1 Postprocess

Fig. 11 shows the postprocess obtained, where the maximum temperature reached in 9,5 seconds can be seen. The maximum temperatures reached are slightly higher than the fusion temperature of the 6063-T5 aluminium.

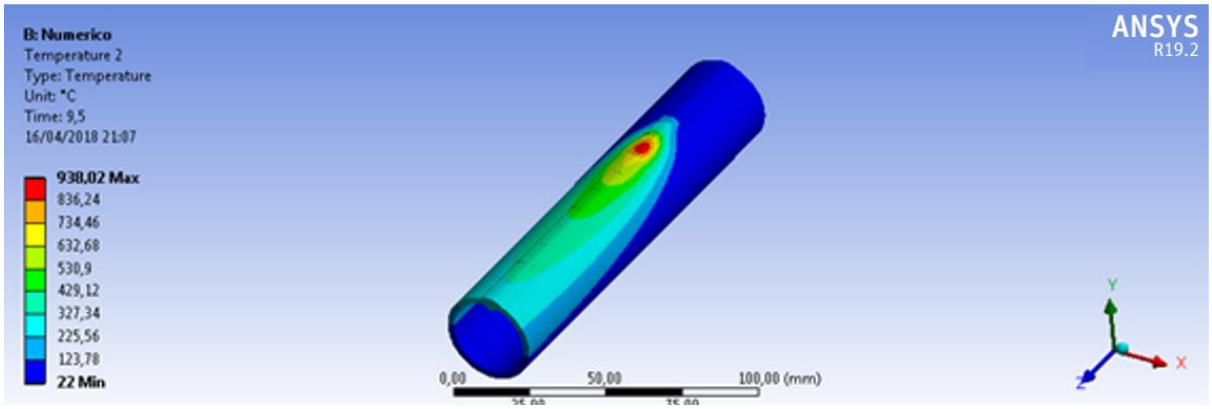

Fig. 11. Postprocess of the numerical simulation

3.4.2 Thermal cycle obtained from the simulation

The curve obtained in the thermal cycle studied is shown below in Fig. 12.

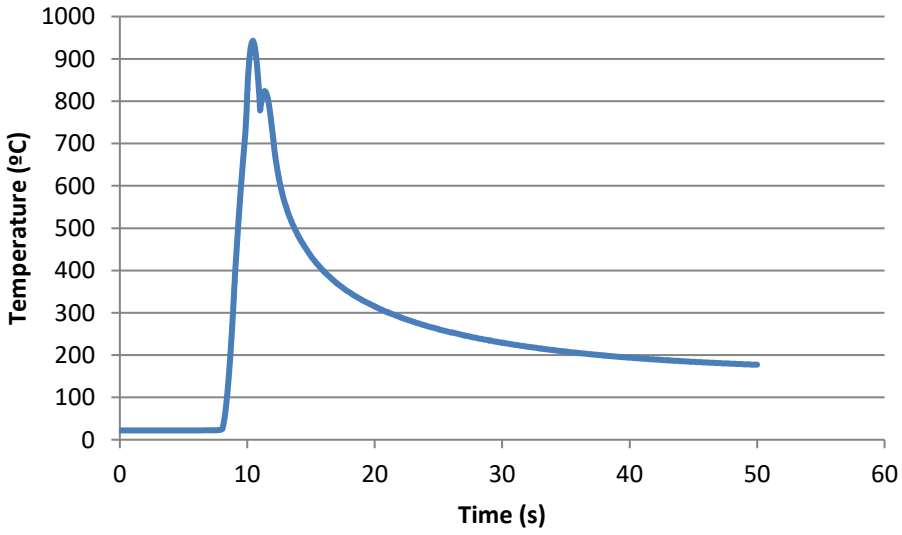

Fig. 12. Welding thermal cycle obtained numerically.

In the simulated welding thermal cycle, readings are taken at the instant of 9,5 seconds and it is observed that the $t_{4/3}$ cooling time is 5,21 seconds.

4. Discussion of the results

The experimental results obtained are compared with the numerical results in Fig. 13.

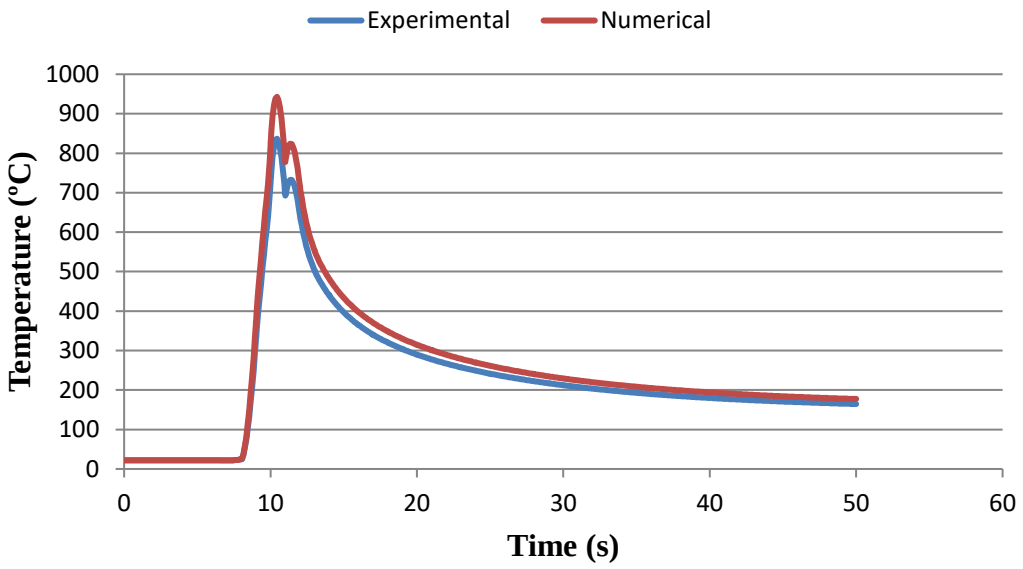

Fig. 13. Comparison between the numerical and experimental thermal cycles

The $t_{4/3}$ cooling time is 4,4 seconds in the experimental study and 5,21 seconds in the numerical one; therefore the accuracy is 85%, which is an acceptable degree of accuracy.

The maximum temperature reached is 837 ºC in the experimental study and 942 ºC in the numerical one; therefore the accuracy between them is 89%, which is an acceptable degree of accuracy.

5. Conclusions

The conclusions that can be drawn from this work are as follows:

- The experimental thermal cycle of the MIG welding process has been numerically validated for the 6063-T5 aluminium alloy from the exact shape of the weld bead obtained experimentally.
- The cooling slope of the welding thermal cycle obtained numerically is very similar to the welding thermal cycle obtained experimentally.
- $t_{4/3}$ has been simulated, obtaining values very similar to those found experimentally.
- The weld bead obtained experimentally has been represented with a high level of accuracy.

6. Nomenclature

NOMENCLATURE	
cp	Specific heat, [J/kgºC]
GTAW	Gas Tungsten Arc Welding
h	Convection coefficient (W/m^{2}ºC)
K	Conductivity [W/mºC]
MIG	Metal Inert Gas
s	Stefan-Boltzmann constant
$t_{4/3}$	Cooling time between 400 ºC and 300 ºC [ºC]
T_∞	Environmental temperatura [ºC]
TTP	Curves of transformation, Temperature–time–property
Greek symbols	
ε	Body surface emissivity

7. References

[1] Boumerzoug, Z., et al., Thermal Cycle Simulation Of Welding Process In Low Carbon Steel, *Mater. Sci. Eng. A*, *530* (2011), pp. 191–195

[2] Sarsilmaz, F., Relationship between micro-structure and mechanical properties of dissimilar aluminum alloy plates by friction stir welding., *Therm. Sci.*, (2018)

[3] Ambriz, R., et al., Effect Of The Weld Thermal Cycles By The Modified Indirect Electric Arc (MIEA) On The Mechanical Properties Of The AA6061-T6 Alloy, *Rev. Metal.*, *45* (2009), 1, pp. 42–51

[4] Ambriz, R.R., et al., Effect Of The Weld Thermal Cycles Of The Modified Indirect Electric Arc On The Mechanical Properties Of The AA6061-T6 Alloy, *Weld. Int.*, *24* (2010), 4, pp. 321–328

[5] Taban, E., et al., Characterization Of 6061-T6 Aluminum Alloy To AISI 1018 Steel Interfaces During Joining And Thermo-Mechanical Conditioning, *Mater. Sci. Eng. A*, *527* (2010), 7-8, pp. 1704–1708

[6] Piris, N., et al., The Influence Of Heat Treatment On Strain Hardening And Strain-Rate Sensitivity Of Aluminium Alloys For Aerospace, *Rev. Metal.*, *40* (2004), 4, pp. 288–293

[7] Polmear, I., et al., *Light Alloys: Metallurgy Of The Light Metals*, Butterworth-Heinemann, 2017

[8] Kassner, M., McMahon, M., The Dislocation Microstructure Of Aluminum, *Metall. Mater. Trans. A*, *18* (1987), 5, pp. 835–846

[9] Shercliff, H., Ashby, M., A Process Model For Age Hardening Of Aluminium Alloys—I. The Model, *Acta Metall. Mater.*, *38* (1990), 10, pp. 1789–1802

[10] Perez, I., et al., Analysis Of The Influence Of Aging Heat Treatment On The Modification Of The Mechanical Properties Of The Alloy AA6060 Processed By ECAE, *Rev. Metal., 47* (2011), 1, pp. 76–89

[11] Croucher, T., Quenching Of Aluminum Alloys: What This Key Step Accomplishes, *Heat Treat., 14* (1982), 5, pp. 20–21

[12] Valdenebro, J.M., et al., Ciclo Térmico Y Soldabilidad De Las Aleaciones De Aluminio, *Rev. Metal., 53* (2017), 3, pp. 103

[13] Cahn, J.W., The Kinetics Of Grain Boundary Nucleated Reactions, *Acta Metall., 4* (1956), 5, pp. 449–459

[14] Miguel, V., et al., Optimización Multiobjetivo Del Proceso De Soldeo GMAW De La Aleación AA 6063-T5 Basado En La Penetración Y En La Zona Afectada Térmicamente, *Rev. Metal., 51* (2015), 1, pp. 037

[15] Meseguer-Valdenebro, J.L., et al., Numerical Study Of TTP Curves Upon Welding Of 6063-T5 Aluminium Alloy And Optimization Of Welding Process Parameters By Taguchi\' S Method, (2017)

[16] Rosenthal, The Theory Of Moving Sources Of And Its Applications To Metal Treatments, *Trans. ASME, 68* (1946), pp. 849-865

[17] Rykalin, R.R., Energy Sources For Welding, *Weld. WORLD*, *12* (1974), 9/10, pp. 272-248

[18] Zeng, Z., et al., Numerical And Experimental Investigation On Temperature Distribution Of The Discontinuous Welding, *Comput. Mater. Sci., 44* (2009), 4, pp. 1153-1162

[19] Guoxiang, X., et al., FINITE ELEMENT ANALYSIS OF TEMPERATURE FIELD IN LASER Plus GMAW HYBRID WELDING FOR T-JOINT OF ALUMINUM ALLOY, *ACTA Metall. Sin., 48* (2012), 9, pp. 1033-1041

[20] Wang, H., et al., Numerical Simulation of the Prestressed Laser Welding of 7075-T7451 Aluminum Alloy Sheet, *Proceedings*, Machining and advanced manufacturing technology x, Laublsrutistr 24, CH-8717 Stafa-Zurich, Switzerland, 2010, Vol. 431-432, pp. 13-16

[21] Alimoradi, A., et al., 3-D Finite Element Simulation of Friction Stir Welding Process of Non Similar Aluminum-Copper Sheets, *Proceedings*, DIFFUSION IN SOLIDS AND LIQUIDS VI, PTS 1 AND 2, Laublsrutistr 24, CH-8717 Stafa-Zurich, Switzerland, 2011, Vol. 312-315, pp. 953-958

[22] Hirasawa, S., et al., Analysis Of Effect Of Tool Geometry On Plastic Flow During Friction Stir Spot Welding Using Particle Method, *J. Mater. Process. Technol., 210* (2010), 11, pp. 1455-1463

[23] Keivani, R., et al., Effects Of Pin Angle And Preheating On Temperature Distribution During Friction Stir Welding Operation, *Trans. Nonferrous Met. Soc. CHINA, 23* (2013), 9, pp. 2708-2713

[24] Zhang, Z., Zhang, H.W., Numerical Studies On Effect Of Axial Pressure In Friction Stir Welding, *Sci. Technol. Weld. Join., 12* (2007), 3, pp. 226-248

[25] Pavelic, V., et al., experimental and computed temperature histories in gas tungsten-arc welding of thin plates, *Weld. J., 48* (1969), 7, pp. S295-

[26] Paley, Z., Hibbert, P., Computation of temperatures in actual weld designs, *Weld. J., 54* (1975), 11, pp. S385-S392

[27] Goldak, J., et al., A New finite-element model for welding heat-sources, *Metall. Trans. B-Process Metall., 15* (1984), 2, pp. 299-305

[28] Meseguer-Valdenebro, J.L., et al., Experimental Validation Of A Numerical Method That Predicts The Size Of The Heat Affected Zone. Optimization Of The Welding Parameters By The Taguchi's Method, *Trans. Indian Inst. Met., 69* (2016), 3, pp. 783-791

[29] Zhu, X.K., Chao, Y.J., Effects Of Temperature-Dependent Material Properties On Welding Simulation, *Comput. Struct., 80* (2002), 11, pp. 967-976

[30] Haupin, W., Aluminum, in: *Encyclopedia of Physical Science and Technology (Third Edition)* (Ed. R.A. Meyers), Academic Press, New York, 2003, pp. 495-518

[31] ***, UNE-EN-287-1. Cualificación de soldadores. Soldeo por fusión. Parte 1: Aceros., AENOR

[32] Mato, P., et al., A Simplified Engineering Method For A T-Joint Welding Simulation, *Therm. Sci., 22* (2018), 3, pp. S867–S873

[33] Deng, D., et al., Numerical Simulation Of Welding Distortion In Large Structures, *Comput. Methods Appl. Mech. Eng., 196* (2007), 45-48, pp. 4613–4627

[34] Segarra, J.A., Portolés, A., Caracterización Microestructural Y Modelización Mediante Elementos Finitos De Uniones Soldadas de la aleación de magnesio AZ31, *Rev. Metal., 54* (2018), 1, pp. 114

[35] Ivanović, I.B., et al., Numerical Study Of Transient Three-Dimensional Heat Conduction Problem With A Moving Heat Source, *Therm. Sci., 15* (2011), 1, pp. 257–266

[36] Bjelić, M.B., et al., Numerical Modeling Of Two-Dimensional Heat-Transfer And Temperature-Based Calibration Using Simulated Annealing Optimization Method: Application To Gas Metal Arc Welding, *Therm. Sci., 20* (2016), 2, pp. 655–665

[37] Meseguer-Valdenebro, J.L., et al., Electrical Parameters Optimisation On Welding Geometry In The 6063-T Alloy Using The Taguchi Methods, *Int. J. Adv. Manuf. Technol., 98* (2018), 9-12, pp. 2449–2460

[38] Fachinotti, V.D., et al., Analytical Solutions Of The Thermal Field Induced By Moving Double-Ellipsoidal And Double-Elliptical Heat Sources In A Semi-Infinite Body, *Int. J. Numer. METHODS Biomed. Eng., 27* (2011), 4, pp. 595-607

[39] Tekelioglu, M., Empirical mapping of the convective heat transfer coefficients with local hot spots on highly conductive surfaces., *Therm. Sci., 21* (2017), 3